Mechano-chemical feedback mediated competition for BMP signalling leads to pattern formation

Daniel J. Toddie-Moore [a],[**],[2], Martti P. Montanari [a],[1], Ngan Vi Tran [b],[1], Evgeniy M. Brik [b], Hanna Antson [b], Isaac Salazar-Ciudad [a],[c],[d], Osamu Shimmi [a],[b],[*]

[a] Institute of Biotechnology, University of Helsinki, 00014, Helsinki, Finland
[b] Institute of Molecular and Cell Biology, University of Tartu, 51010, Tartu, Estonia
[c] Genomics, Bioinformatics and Evolution. Department de Genètica I Microbiologia, Universitat Autònoma de Barcelona, 08193, Cerdanyola Del Vallès, Spain
[d] Centre de Rercerca Matemàtica, 08193, Cerdanyola Del Vallès, Spain

ABSTRACT

Developmental patterning is thought to be regulated by conserved signalling pathways. Initial patterns are often broad before refining to only those cells that commit to a particular fate. However, the mechanisms by which pattern refinement takes place remain to be addressed. Using the posterior crossvein (PCV) of the *Drosophila* pupal wing as a model, into which bone morphogenetic protein (BMP) ligand is extracellularly transported to instruct vein patterning, we investigate how pattern refinement is regulated. We found that BMP signalling induces apical enrichment of Myosin II in developing crossvein cells to regulate apical constriction. Live imaging of cellular behaviour indicates that changes in cell shape are dynamic and transient, only being maintained in those cells that retain vein fate competence after refinement. Disrupting cell shape changes throughout the PCV inhibits pattern refinement. In contrast, disrupting cell shape in only a subset of vein cells can result in a loss of BMP signalling. We propose that mechano-chemical feedback leads to competition for the developmental signal which plays a critical role in pattern refinement.

1. Introduction

Pattern formation is a fundamental process in animal development, for which various molecular mechanisms have been proposed, including gene regulatory networks and growth factor signalling (Morelli et al., 2012; Schweisguth and Corson, 2019). Developmental patterning often involves refinement from a broad initial area of competency for a fate to only those cells that commit to it, with neighbours losing competence and following an alternate fate path (Fig. 1A) (Morelli et al., 2012; Schweisguth and Corson, 2019). Whilst some mechanisms of pattern refinement, such as transcriptional networks and lateral inhibition, have previously been investigated, the role played by diffusible growth factor signalling, in particular the interactions between signalling and morphogenesis, has been less explored (Gilmour et al., 2017; Hannezo and Heisenberg, 2019).

The posterior crossvein (PCV) of the *Drosophila* pupal wing serves as

an excellent model to address the dynamics of signalling and morphogenesis, as its formation is initially directed by a single signalling pathway: Bone morphogenetic protein (BMP) signalling (Matsuda et al., 2013; Ralston and Blair, 2005). The *Drosophila* BMP ligand Decapentaplegic (Dpp) is initially expressed in the adjacent longitudinal veins (LVs) and is extracellularly transported into the prospective PCV region along the basal surfaces of the two cell layers that comprise the wing epithelia (Fig. 1B) (Matsuda and Shimmi, 2012). Extracellular transport at this stage requires the BMP binding proteins Short gastrulation (Sog) and Crossveinless (Cv), which bind to the Dpp ligand and facilitate its active transport into the PCV region (Shimmi and Newfeld, 2013; Shimmi et al., 2005).

BMP signalling induced by the Dpp ligand forms the PCV field, directing cells to become competent for vein fate, rather than the intervein fate that occurs if BMP signalling is not activated or is not sustained (Fig. 1C) (Ralston and Blair, 2005; Shimmi et al., 2005). Continuous
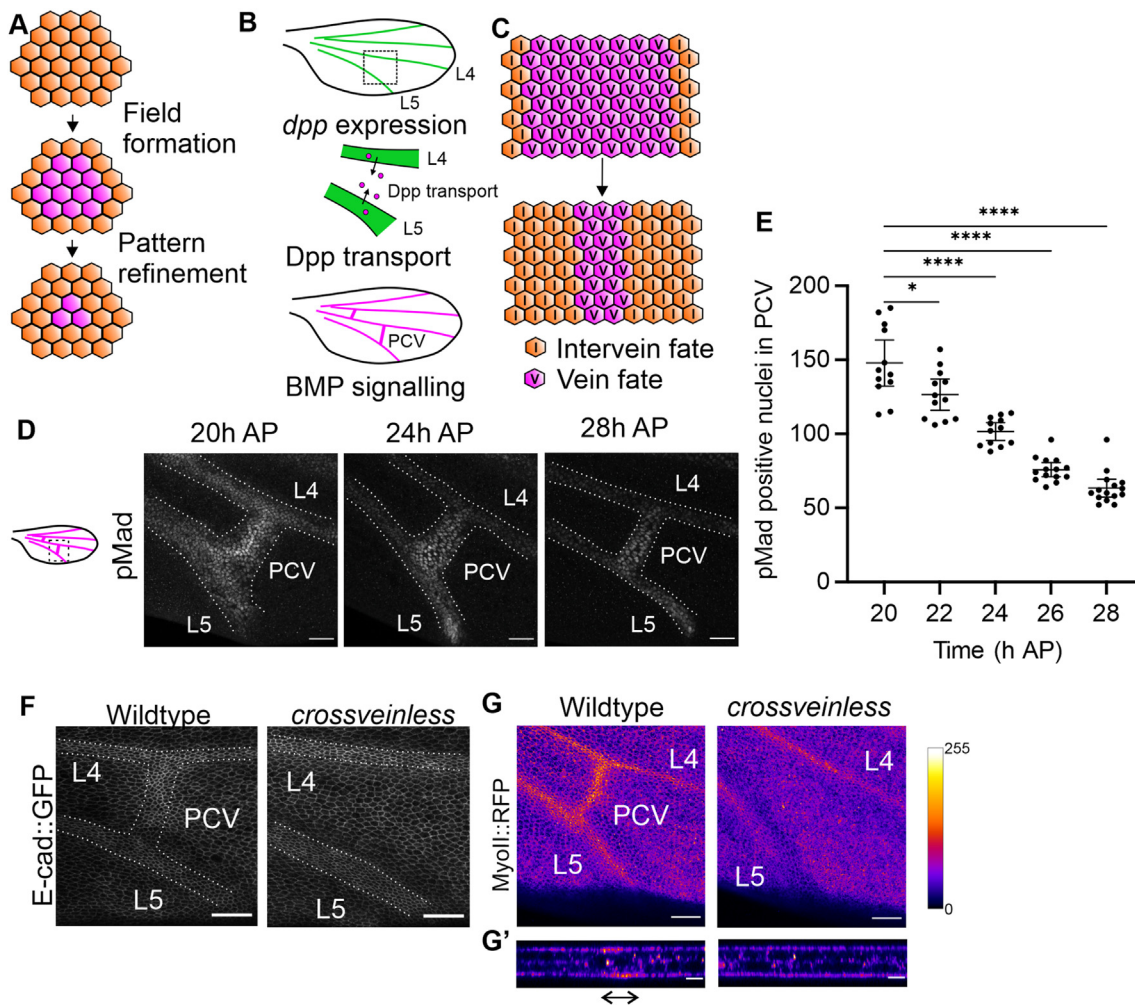
Fig. 1. The PCV field refines during vein patterning and morphogenesis. (A) Schematic depicting the refinement of developmental patterns from an initial field to cells committing to a fate. (B) The expression and signalling pattern of the BMP ligand Dpp in the developing pupal wing. L4, L5, and PCV denote longitudinal veins 4, 5, and posterior crossvein, respectively. Top: *dpp* mRNA (green) is expressed in longitudinal veins, but not in crossveins, during early pupal stages. Middle: Schematic model of Dpp/BMP ligand transport from the longitudinal veins into PCV. Bottom: BMP signalling (magenta) is detected at all wing vein primordia including longitudinal veins and crossveins. (C) Schematic depicting the refinement of the BMP signalling pattern in the PCV field. (D) BMP signalling (shown by pMad) in the PCV field of wild type pupal wings at 20 h, 24 h and 28 h AP. Left: Schematic of pupal wing. Approximate position of imaging is shown as a square. Median filter applied. Dashed lines depict boundary of vein cells. (E) The number of cells in which BMP signalling is occurring during the refinement period. Sample sizes are 12 (20 h), 12 (22 h), 12 (24 h), 14 (26 h) and 15 (28 h). *$P = 0.0207$, ****$P < 0.0001$. Data are means ± 95 % confidence intervals (CIs). Statistical significance was calculated by the two-tailed *t*-test. (F) E-cad::GFP in the PCV region in wild type (left) and *crossveinless* mutant (right) pupal wings at 24 h AP. Apical cell shapes are highlighted by max composite of E-cad:GFP. Dashed lines depict approximate boundary of vein cells. (G) Heatmap of the apical intensity of MyoII::RFP in cells of the PCV region in wild type (left) and *crossveinless* mutant (right) pupal wings at 24h AP. Optical cross sections on the PCV region are shown at the lower panel (G′). Prospective PCV position is indicated by double-headed arrow. The apical distribution of MyoII is shown through the PCV region. Scale bars: 25 μm for D, F and G, and 10 μm for G'.

extracellular Dpp transport seems to be crucial for a period of around 10 h (18–28 h after pupariation (AP)) to maintain the PCV field and vein fate competence, before PCV cells begin to express the ligand themselves (Ralston and Blair, 2005). Continued extracellular signalling and vein morphogenesis occur concurrently, as morphogenesis begins shortly after BMP signalling is activated (Matsuda et al., 2013). Refinement of the BMP signalling pattern during this time window has previously been observed; however, how pattern refinement takes place has not been addressed (Gui et al., 2016).

In this study, to understand how refinement of the BMP signalling pattern takes place during PCV fate determination, we utilized *Drosophila* genetics and *in vivo* live imaging. Our data reveal a mechano-chemical feedback loop that drives competition between cells for BMP signalling leading to pattern refinement.

2. Materials and methods

2.1. Fly genetics

UAS-mCD8::GFP (#5137), *en-Gal4* (#30564), and UAS-MBS.N300 (#63791) were obtained from the Bloomington *Drosophila* Stock Centre. *UAS-tkv^{Q253D}* and *cv^{70}* were described previously (Gui et al., 2016; Shimmi et al., 2005). *E-cad::GFP* was obtained from H. Ohkura (Shimada et al., 2006), *MyoII::RFP* from R. Le Borgne (Daniel et al., 2018), *UAS-MyoII-DN* from D. Kiehart (Franke et al., 2005), and *sqh-GAP43::mCherry* from A. Martin (Rauzi et al., 2010). Populations of mixed sex were used except for when using *yw* or *tubP-Gal80^{ts}* on X, where females were selected, and experiments involving *crossveinless*, where only males were used. The ages of pupal wings at dissection are given at developmental timepoints equivalent to 25°C. Calculations for relative developmental timing at 18°C, 25°C and 29°C were based on previously published data and rounded to the nearest hour (Ashburner

et al., 2004). For experiments using *en-Gal4*, pupae were raised at 18 °C for 22 h after pupariation, and then shifted to 29 °C for 10 (Fig. 3B, C, D, E, Supplemental Fig. 2A) or 12 (Supplemental Figs. 3B and C) hours before dissection and fixation. The exception to this was the experiment involving *UAS-MBS.N300*, when pupae were raised at 29 °C for 21 h after pupariation (Supplemental Fig. 2B). For clone generation, larvae were raised at 25 °C for 3–4 days after egg laying (AEL) (or 18 °C for 6–7 days AEL), before being heat shocked in a 37 °C water bath for 1 h. Vials containing larvae were then placed at 18 °C until at the white pre-pupal stage, and then transferred to 29 °C for 21 h before dissection and fixation (Fig. 3G, I, Supplemental Figs. 1B and 2D). For time-lapse imaging, pupae were raised at 25 °C until 17 h after the pre-pupal stage. They were then moved to room temperature for 1 h, during which windows were cut into the pupal case and pupae mounted, before being imaged as previously described (Gui et al., 2019).

2.2. Full genotypes

Fig. 1D and E, Fig. 2F, Fig. 4A–C, E-G, and Supplemental Fig. 3A: *yw*.

Fig. 1F: *yw; ubi-E-cad::GFP*, or *cv70; ubi-E-cad::GFP*.

Fig. 1G and Supplemental Fig. 1A: *MyoII::RFP*, or *MyoII::RFP, cv70*

Fig. 2A–C and Supplemental Videos 1–3: *ubi-E-cad::GFP/sqh-Gap43::mCherry*.

Fig. 3B–F: *en-Gal4/UAS-mCD8::GFP; tubP-Gal80^{ts}*, or *en-Gal4/UAS-MyoII-DN; tubP-Gal80^{ts}*

Fig. 3G and Supplemental Fig. 2D: *hs-Flp; tubP-Gal4 UAS-mCD8::GFP/ UAS-MyoII-DN; tubP-Gal80 FRT^{82B} /FRT^{82B}*

Fig. 3I: *hs-Flp; tubP-Gal4 UAS-mCD8::GFP/UAS-tkv^{Q253D}; FRT^{82B} tubP-Gal80/FRT^{82B}*

Supplemental Fig. 1B: *hs-Flp/tubP-Gal80^{ts}, MyoII::RFP; tubP-Gal4 UAS-mCD8::GFP/UAS- tkv^{Q253D}; tubP-Gal80 FRT^{82B} /FRT^{82B}*

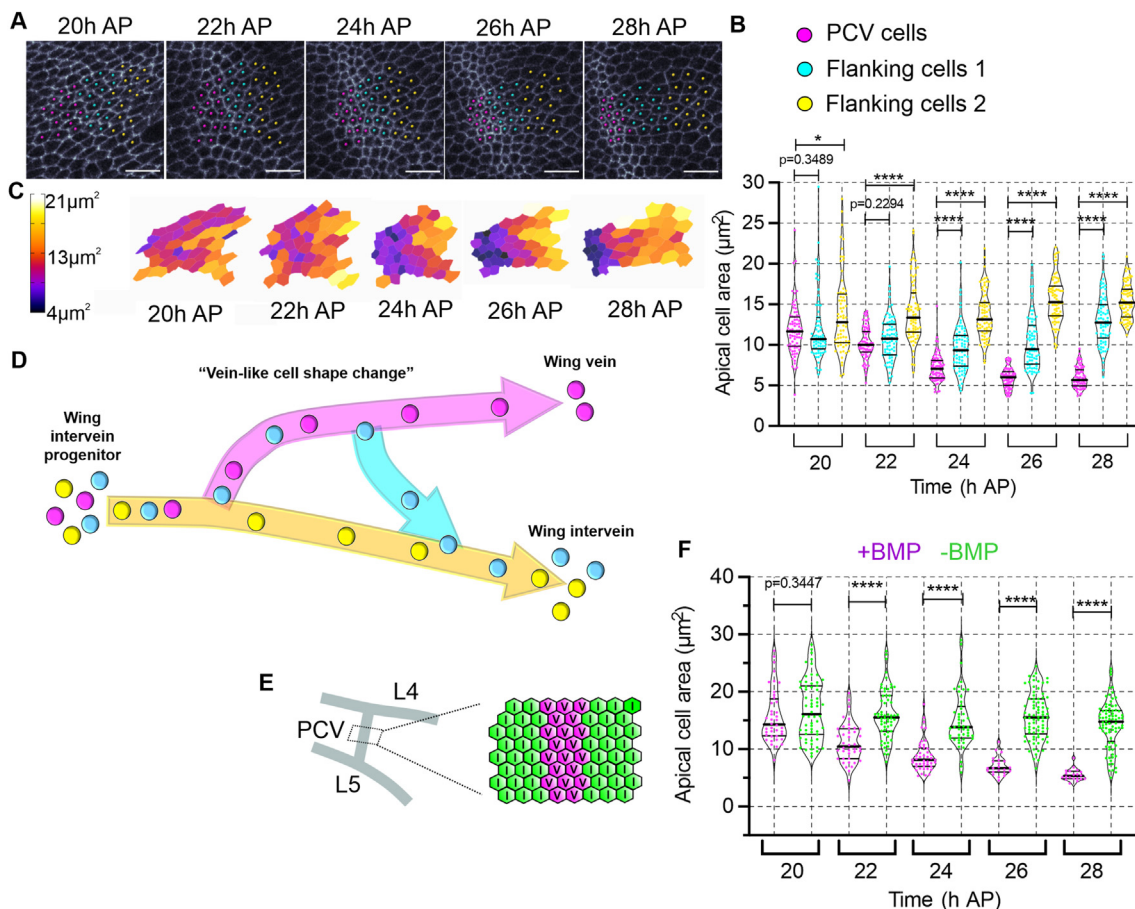Supplemental Fig. 2A: *cv70; en-Gal4/+; tubP-Gal80^{ts}*, or *cv70; en-Gal4/*

Fig. 2. Changes in cell shape are dynamic and transient during pattern refinement. (A) Time-lapse images of E-cad::GFP in the PCV region at 20 h, 22 h, 24 h, 26 h and 28 h AP. Three clusters of cells are marked. Future PCV cells (magenta) show progressive apical constriction. Cells immediately adjacent to future PCV cells (cyan) show transient apical constriction at 22 h, 24 h and 26 h AP before reverting to an intervein-like structure. Cells further from future PCV cells (yellow) do not show apical constriction. PCV cells are categorised by their shape at 28 h AP and flanking categories by their relative position and shape at 28 h AP. Scale bars: 10 μm. (B) Apical size of PCV cells and their neighbours during the refinement period. N=75 cells per category (15 cells tracked per category in each wing, for 5 wings). Violin plots show median, and 25th and 75th percentiles. Data from five independent time-lapse images. Each data point [PCV cells: magenta, cells adjacent to PCV (Flanking cells 1): cyan, cells further from PCV (Flanking cells 2): yellow] represents one cell. *$P = 0.0185$, ****$P < 0.0001$. Data were analysed by two-sided Mann-Whitney U test. (C) Heat map showing the changes in apical area of cells of the PCV field. The heatmap was produced using the ROI colour coder plugin, part of the BAR collection of ImageJ. The same cells are shown as in A. (D) Schematic of changes in fate path during PCV patterning. Cells that are initially a vein-like cell shape (cyan) lose competence during patterning, and move outside of the vein fate path (magenta) into the intervein fate path (yellow). (E) Schematic of PCV field. Approximate position of cell area within (V) and outside of (I) the PCV field is shown as a box (left). Schematic of cells within (magenta) and outside of (green) PCV field during the refinement period (right). (F) Apical surface areas of cells within and outside of the PCV field during the refinement period. Cells measured from images of fixed wings stained with Dlg1, pMad and F-actin. Sample sizes (from 5 wings) are 40 (20 h + BMP), 60 (20 h –BMP), 40 (22 h + BMP), 60 (22 h –BMP), 44 (24 h + BMP), 48 (24 h –BMP), 22 (26 h + BMP), 80 (24 h –BMP), 20 (28 h + BMP) and 79 (28 h –BMP). Violin plots show median, and 25th and 75th percentiles. Data from five independent images. Each data point [cells within the PCV (magenta); cells outside of the PCV (green)] represents one cell. ****$P < 0.0001$. Data were analysed by two-sided Mann-Whitney U test.
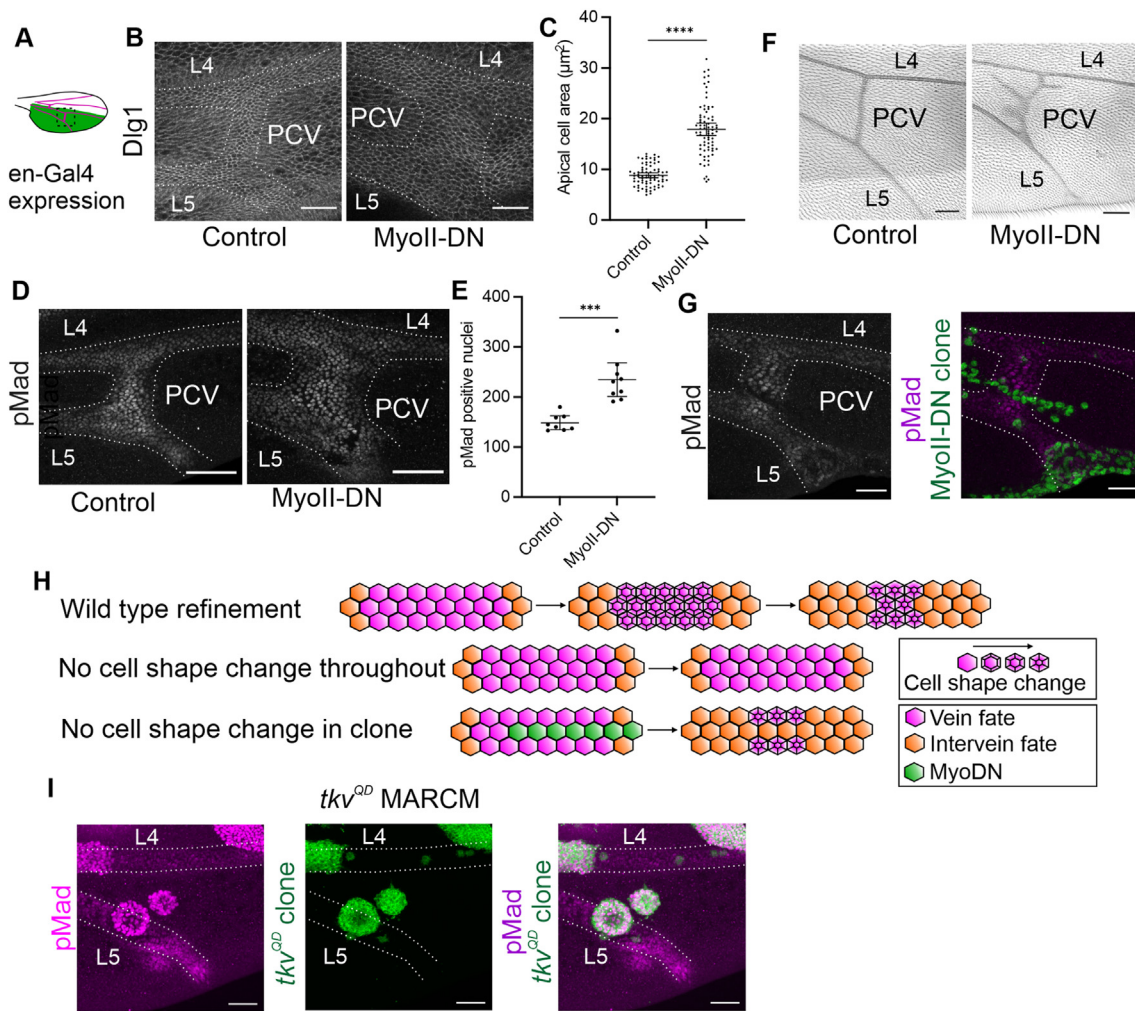
Fig. 3. Loss of MyoII activity has context-specific effects on BMP signalling pattern refinement. (A) Schematic of pupal wing. Posterior region of the wing and Engrailed-Gal4 expression pattern is shown in green. Approximate position of imaging is shown as a square (dotted outline). (B) Apical cell shape (Dlg1) in the PCV region in control (left, *en > mCD8::GFP*) and MyoII attenuated pupal wings (right, *en > MyoII-DN*) at 23 h AP. MyoII-DN was expressed throughout the posterior wing by *en-gal4* for 10 h prior to dissection. (C) Apical size of cells in which BMP signalling is occurring (and thus are within the PCV field) in the PCV of 23h AP pupal wings. N=75 cells per category (15 cells in each wing, for 5 wings). ****$P < 0.0001$. Data are means ± 95 % confidence intervals (CIs). Statistical significance was calculated by the two-tailed *t*-test. (D) pMad expression in the PCV region in control (left, *en > mCD8::GFP*) and MyoII attenuated pupal wings (right, *en > MyoII-DN*) at 23 h AP. MyoII-DN was expressed throughout the posterior wing by *en-gal4* for 10 h prior to dissection. Median filter applied. (E) Number of cells in which BMP signalling is occurring (and thus are within the PCV field) in the PCV of 23h AP pupal wings. N = 8 (control) and 9 (MyoII-DN). ***$P = 0.0001$. Data are means ± 95 % confidence intervals (CIs). Statistical significance was calculated by the two-tailed *t*-test. (F) Adult wings in the PCV region in control (left, *en > mCD8::GFP*) and MyoII attenuated pupal wings (right, *en > MyoII-DN*). (G) Effects of clonal expression of MyoII-DN within a subset of cells of the PCV field. pMad staining alone (white, left), or pMad staining (magenta), MyoII-DN expressing clones (green) at 25 h AP (right). Median filter applied to pMad staining. (H) Top: Schematic depicting model of wild type pattern refinement whereby loss of cell shape changes from cells at the edge of the PCV field results in their exclusion from the field (by loss of BMP signalling and thus cell fate). Middle: Loss of MyoII activity and cell shape change throughout the PCV blocks refinement. Bottom: Loss of MyoII activity in a subset of PCV cells can lead to loss of signal and fate (ectopic refinement). (I) Effects of clonal expression of Tkv^QD within a subset of cells of the PCV field. pMad staining alone (magenta, left), or pMad staining (magenta) Tkv^QD-expressing clones (green) at 25 h AP (right). Median filter applied to pMad staining. Dashed lines depict boundary of vein cells. Scale bars: 50 μm for B, D, F, I and 25 μm for G.

UAS-MyoII-DN; tubP-Gal80^ts

Supplemental Figs. 2B and C: *en-gal4/+; UAS- mbs.N300/tubP-Gal80^ts or en-gal4/UAS-mCD8:GFP; tubP-Gal80^ts*

Supplemental Figs. 3B and C: *en-gal4/sqh-Gap43::mCherry; tubP-Gal80^ts, or en-gal4/UAS-MyoII-DN, sqh-Gap43::mCherry; tubP-Gal80^ts*

2.3. Immunohistochemistry

Pupae were fixed in 3.7% formaldehyde (Sigma-Aldrich) for two nights at 4 °C before dissecting the pupal wings and blocking with Normal Goat Serum (10%) overnight. Both primary and secondary antibody incubations also took place overnight at 4 °C. The following primary antibodies were used: mouse anti-DLG1 [1:40; Developmental Studies Hybridoma Bank (DSHB), University of Iowa] and rabbit anti-phospho-SMAD1/5 (1:200; Cell Signalling Technologies). Secondary antibodies were anti-rabbit IgG Alexa 568 (1:200, Invitrogen), anti-mouse IgG Alexa 647 (1:200; Life technologies), anti-rabbit IgG Alexa 647 (1:200; Life technologies). F-actin was stained with Alexa 488-conjugated phalloidin (1:200; Life technologies).

2.4. Imaging and Image analysis

Confocal images and time-lapse images were acquired using a Leica SP8 STED confocal microscope. Time-lapse images were processed using Imaris v9.1.2 (Bitplane/Oxford Instruments) and snapshots segmented by hand in Image J/Fiji (v. 1.52p and 1.53c) (Schindelin et al., 2012). All
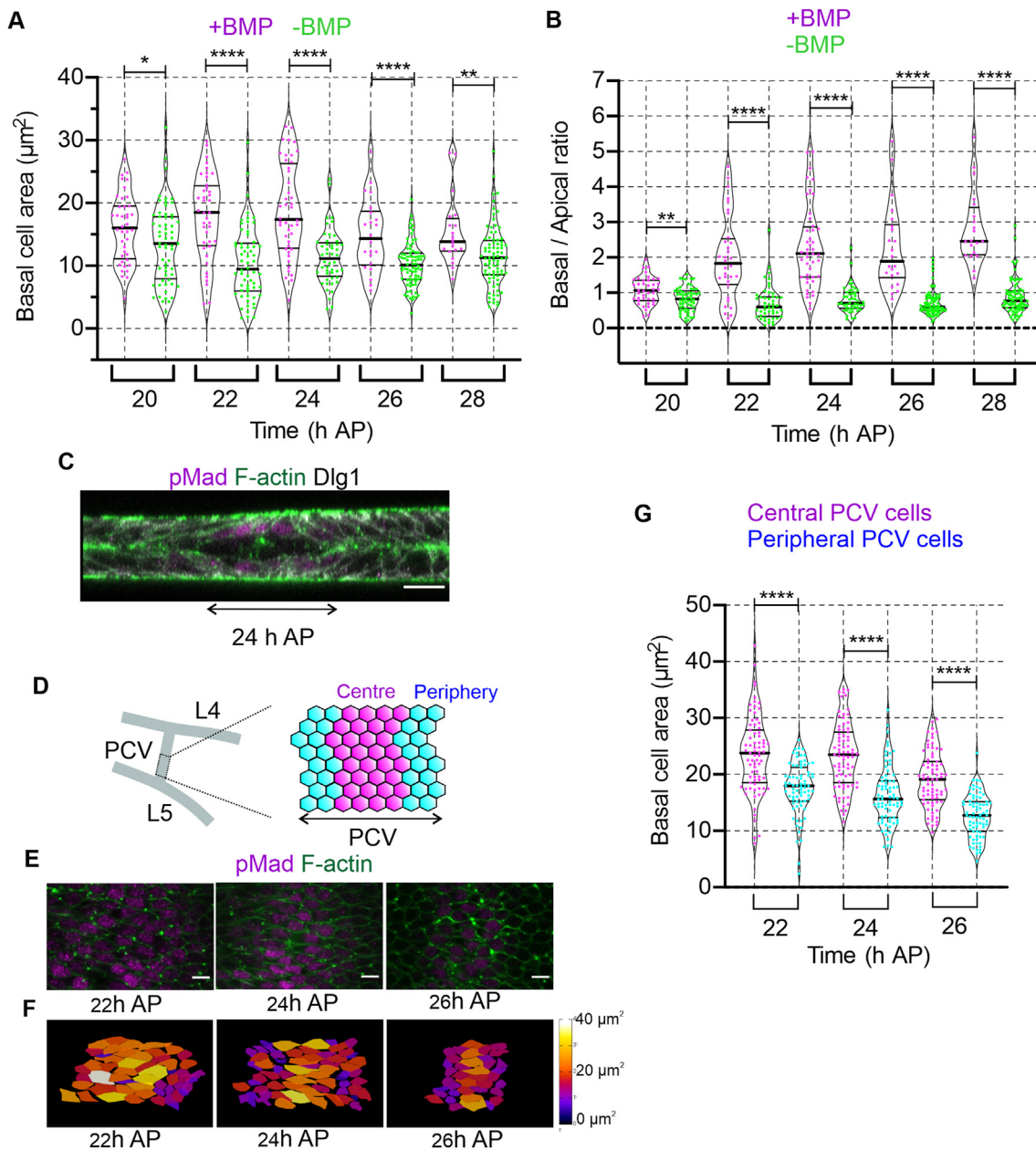
Fig. 4. BMP signal induces basal expansion in the PCV field during PCV morphogenesis. (A) Basal surface areas of cells within and outside of the PCV field during the refinement period. Sample sizes (from 5 wings) are 40 (20 h + BMP), 60 (20 h –BMP), 40 (22 h + BMP), 60 (22 h –BMP), 44 (24 h + BMP), 48 (24 h –BMP), 22 (26 h + BMP), 80 (24 h –BMP), 20 (28 h + BMP) and 79 (28 h –BMP). Violin plots show median, and 25th and 75th percentiles. Data from five independent images. The same cells were measured as in Fig. 2F. Each data point [cells within the PCV (magenta); cells outside of the PCV (green)] represents one cell. *$P = 0.0329$, **$P = 0.0037$, ****$P < 0.0001$. Data were analysed by two-sided Mann-Whitney U test. (B) Ratio of basal and apical surface of cells in Figs. 2F and 4A. Each data point [cells within the PCV (magenta) and cells outside of the PCV (green)] represents one cell. **$P = 0.0030$, ****$P < 0.0001$. Data were analysed by two-sided Mann-Whitney U test. (C) Optical cross section focused on the PCV region showing pMad (magenta) Dlg1 (white) and F-actin (green) at 24 h. Prospective PCV position is indicated by double-headed arrows. (D) Schematic of PCV field. Approximate position of cell area within the PCV field is shown as a box (left). Schematic showing position of cells termed both central (magenta) and peripheral (cyan) within the PCV field during the refinement period (right). (E) Max composites showing basal cell shape of PCV field cells at the level of central PCV cell basal surface during the refinement period. pMad staining (magenta) and F-actin (green) at 22h, 24h and 26h AP. Median filter applied to pMad staining. (F) Heat map showing the basal cell areas of cells within the PCV field. The heatmap was produced using the ROI colour coder plugin, part of the BAR collection of ImageJ. (G) Basal cell areas of peripheral and central PCV cells during refinement. N = 75 (15 cells per wing, data from 5 wings pooled). Violin plots show median, and 25th and 75th percentiles. Each data point (central PCV cells: magenta, peripheral PCV cells: cyan) represents one cell. ****$P < 0.0001$. Data were analysed by two-sided Mann-Whitney U test. The same wings are analysed for Fig. 2F and all of Fig. 4. Scale bars: 10 μm for C and 5 μm for E.

other images were processed and analysed using Fiji. All images (with the exception of cross sections), including time-lapse snapshots, are maximum composites. A median filter was applied to pMad images in Fiji. Cell size heatmaps were generated using the ROI colour coder plugin, part of the BAR collection of ImageJ (Ferreira et al., 2017).

The number of pMad-positive cells within the PCV field was calculated by first excluding adjacent LV nuclei by marking the predicted trajectory of the LV–PCV boundary by drawing across from the edge of L4 and L5 on either side of the PCV. pMad-positive nuclei between these lines were then counted. Z projections of median filtered images were

used for quantification, using the stacks for reference.

The apical and basal sizes of field cells were analysed using individual slices of stacks in Fiji. Cells that showed pMad staining in the nucleus were traced and measured. The most apical or basal slice where the cell outline was clear was used for each cell. Cells at the centre and posterior portion of the PCV were analysed. Cells in the middle 50% of the PCV (as indicated by pMad) were designated central cells and those outside this peripheral.

Cell volumes were determined for the same cells for which apical and basal surface areas had been measured. To measure cell volumes, the RoiManager3D tool was used, a plug-in in the 3D ImageJ Suite (version 3.96) (Ollion et al., 2013).

All representative images are representative of at least three biological replicates.

Fig. 1G and Supplemental Fig. 1A were generated from the same stacks. Fig. 2A, C and Supplemental Videos 1–3 show the same cells, and are from the data set quantified in Fig. 2B. Figs. 2F and 4 and Supplemental Fig. 3A represent analyses and images of the same data set, with Figs. 2F and 4A, B and Supplemental Fig. 3A analysing the same cells.

All images are representative of at least three biological replicates.

2.5. Statistics

Statistical analyses were performed using GraphPad Prism software (v.8.3.0, GraphPad). The number for all quantified data is indicated in the figure legends.

Figs. 1E and 3C, E: data are means $\pm$ 95 % confidence intervals (CIs). Statistical significance was calculated by the two-tailed *t*-test method.

In other figures, *P* values were calculated using a two-sided Mann-Whitney test and specified in the figure legends and in the corresponding plots.

3. Results

3.1. BMP signalling induces cell shape changes during pattern refinement

First, we confirmed that refinement of the PCV field takes place during PCV morphogenesis. The PCV field is defined as the cells in which BMP signalling occurs, as indicated by staining with anti-phosphorylated Mad antibody (pMad) (Ross et al., 2001), and which are therefore competent to assume a vein fate. Our data reveal that the number of cells within the PCV field reduces between 20h AP, shortly after the initiation of PCV patterning, and 28h AP, when PCV cells express *dpp* themselves (Fig. 1D and E). Thus, we term the period from 20 to 28 h AP the 'refinement period'.

During this period, apical constriction of vein cells appears to be the hallmark of vein morphogenesis (Fristrom et al., 1993; Gui et al., 2016; Maartens, 2012). Since BMP signalling is thought to initiate PCV development (Matsuda and Shimmi, 2012), we next asked whether BMP signalling directs the wing vein-like cell shape changes (hereafter referred to as "cell shape changes") that occur during PCV morphogenesis. To answer this question, we captured images of apical cell shapes in the PCV region of *crossveinless* mutant wings, into which Dpp cannot be transported, and where BMP signalling is thus inactive. We observed that apical constriction does not occur where the PCV normally forms (Fig. 1F) (Shimmi et al., 2005), indicating that BMP signalling is required for the cell shape changes that occur during PCV morphogenesis.

The activity of Myosin II (MyoII) has been proposed to be the driving force behind cell shape dynamics such as apical constriction (Martin and Goldstein, 2014). To investigate whether BMP signalling directs cell shape change through MyoII activity, we analysed the spatial localisation of MyoII using MyoII regulatory light chain (MRLC) tagged with RFP in wild type and *crossveinless* pupal wings (Daniel et al., 2018). In wild type wings, MyoII is enriched in the apical compartment of PCV cells, with lower basal levels, but in contrast, neighbouring intervein cells have lower apical levels of MyoII than the PCV (Fig. 1G, Supplemental

Fig. 1A). Conversely, in *crossveinless* pupal wings, apical MyoII enrichment is not observed in the PCV region, although apical enrichment of MyoII is still detected in LVs (Fig. 1G, Supplemental Fig. 1A). These findings suggest that BMP signalling facilitates the apical localisation of MyoII to promote apical constriction of PCV cells. This was further confirmed by the observation that ectopic expression of the constitutively active form of BMP type I receptor Thickveins (Tkv^{QD}) in mosaic analysis with a repressible cell marker (MARCM) clones within the pupal wing induces apical enrichment of MyoII and apical constriction (Supplemental Fig. 1B) (Gui et al., 2016; Lee and Luo, 1999).

3.2. Time lapse imaging during PCV morphogenesis reveals reversible fate path

As wing vein morphogenesis directed by BMP signalling and refinement of the BMP signalling pattern occur concurrently, we hypothesised that these events could be mutually coordinated. To address this, we employed *in vivo* live imaging of pupal wings expressing GFP-tagged E-cadherin (E-cad::GFP) to observe cell shape changes during the refinement period (Shimada et al., 2006). We tracked the apical shapes of cells that are part of the PCV at the end of the refinement period, and thus retained vein fate competence, and compared them to the cells flanking this region (Fig. 2A–C, Supplemental Videos 1–3). Intriguingly, whilst the cells that will form the PCV constrict apically throughout the refinement period, several of the cells immediately flanking these constrict apically at early time points, but fail to maintain their vein-like morphology at later time points, eventually reverting to an intervein-like shape (Fig. 2A–D, Supplemental Videos 1 and 2). We next sought to observe whether these cells losing their apically constricted shape was linked to their BMP signalling state by examining cell shapes both within and outside of the PCV field throughout refinement (Fig. 2 E, F). We observe that PCV field cells (positive for BMP signalling) are constricted throughout refinement, whereas flanking intervein cells are not. As the field progressively refines during this period, flanking cells at later time points would have earlier been part of the field. Therefore, the BMP signalling state, and thus fate competence, of these cells is also transient and reversible, and coupled to transient and reversible cell shape changes.

3.3. Cell shape change and pattern refinement are coupled

We hypothesised that cell shape changes themselves may affect signalling pattern refinement and thus cell fate choice in the PCV region. To test this idea, we modulated cell shape changes in the developing wing by attenuating MyoII activity, using a dominant negative form of the Myosin Heavy Chain (MyoII-DN) (Franke et al., 2005). Inhibiting MyoII activity across the posterior wing blade for 10 h during PCV morphogenesis is sufficient to disrupt apical constriction in the PCV region and LV cells of 23h AP pupal wings (Fig. 3A–C). Intriguingly, loss of MyoII activity throughout the posterior wing results in a broader range of BMP signalling in the PCV region than in control wings, suggesting that cell shape changes are necessary for the refinement of the BMP signalling pattern, but not for BMP signalling itself (Fig. 3D and E). Consistently, adult wings show disrupted PCV patterning, manifesting both as vein thickenings and branches that extend from the normally straight PCV, suggesting that the organisation of cell fates has been disrupted (Fig. 3F). Additionally, BMP signalling was missing in the PCV region when MyoII activity was disrupted in the posterior half of *crossveinless* wings, indicating that the unrefined BMP signalling pattern is still being directed by extracellular BMP signalling (Supplemental Fig. 2A). We further confirmed that dynamic MyoII activity is crucial for refinement of BMP signalling using the ectopic expression of constitutively active Myosin binding subunit (Mbs), a regulatory subunit of myosin phosphatase, which also leads to a broader range of BMP signalling in the PCV region (Supplemental Figs. 2B and C) (Mitonaka et al., 2007). These findings indicate that a self-organising mechano-chemical loop occurs during crossvein

patterning as the BMP signal induces apical Myosin II localisation to instruct cell shape changes, the activity of which is necessary for the proper patterning of the BMP signal which directs it.

3.4. Competition for BMP signalling takes place at the PCV region

What then is the role of cell shape changes in signalling pattern refinement? Despite reversal of BMP-induced cell shape changes being associated with reduced competence for vein fate, blocking cell shape changes did not affect BMP signalling. We hypothesised that what might be important is not cell shape change itself, but how cell morphology compares to that of other cells within the field. The impact of cell shape change loss may then be context-specific, facilitating refinement by causing less signalling and subsequent fate loss in cells surrounded by those more readily able to change shape. If this is the case, inhibition of cell shape changes in a small group of cells within the PCV field may decrease their ability to retain BMP signalling and vein fate. We tested this hypothesis by generating clones that attenuate cell shape changes amongst neighbours that are wild type. Strikingly, when small MyoII-attenuated clones are produced within the PCV field, loss of BMP signalling can often be observed in a context-dependent manner (Fig. 3G). Larger clones expressing Myo-DN displayed a lack of refinement, similar to when Myo-DN is expressed throughout the posterior wing blade (Supplemental Fig. 2D). This suggests that MyoII-based cell shape changes play a crucial role in whether a cell retains vein fate during refinement, despite these shape changes not being required for BMP signalling. When all or many neighbouring PCV field cells cannot form vein-like shapes, signalling still occurs, and refinement does not take place (Fig. 3A–E, H, Supplemental Fig. 2D). However, when cells are present in a heterogeneous population, with or without cell shape changes, only cells that can change shape both retain the signal and acquire vein fate (Fig. 3G and H). We propose that cells of the PCV field may be competing for BMP signalling via their changes in cell shape, with those that can change and retain vein-like shapes being more readily able to retain BMP signalling than their neighbours. Furthermore, our data indicate that the self-organising MyoII-BMP mechano-chemical feedback loop is the mechanism by which pattern refinement occurs at the PCV; with BMP signalling inducing the cell shape changes, which in turn influence the ability of cells to retain that signal.

As BMP-signalling-induced cellular changes appear to be needed for the refinement of the signal itself, we further considered that stronger signalling may make cells more competitive for receiving the signal. Therefore, we generated clones of the constitutive active form of the BMP type I receptor (Tkv^{QD}) to examine whether increasing BMP signalling beyond wild type levels could generate super-competitive cells. Cells within these clones displayed strong BMP signalling and were apically constricted, indicating enhancement of the cellular processes downstream of BMP signalling. Strikingly, inducing tkv^{QD} clones in wings can cause non-autonomous loss of the pMad signal at the PCV region, but not in LVs (Fig. 3I), suggesting that cells expressing Tkv^{QD} do become super-competitive for BMP signalling for PCV fate induction in a non-autonomous manner. This strongly supports the hypothesis that cells compete for BMP signalling in the PCV field, and that high levels of signalling in some cells are able to perturb signalling in others.

3.5. Basal cell shape is a potential mechanism of competition between cells

We next considered what the mechanism of competition between cells for the BMP signal is, and how cell shape might play a role. Expansion of the basal domain of cells has often previously been observed when apical constriction occurs and cells retain their volume (Kondo and Hayashi, 2015). Furthermore, basal expansion of vein cells could be an important step in vein morphogenesis in a system where a lumen needs to form but the tissue does not fold. Previous findings indicate that extracellularly trafficked Dpp ligands are predominantly localised on the basal side of the wing epithelia (Matsuda and Shimmi,

2012), therefore basal expansion could increase a cell's competence for the basally localised ligand.

To investigate whether PCV field cells basally expand, we compared the basal sizes of BMP positive and negative cells at timepoints during the refinement period (Fig. 4A). We observe that as cells within the PCV field (BMP signal positive) apically constrict, they also basally expand, unlike cells outside of the PCV field (BMP signal negative) (Figs. 2F, 4A-C). Since the volume of cells is largely conserved throughout the refinement period (Supplemental Fig. 3A), it appears that basal expansion is induced by BMP-induced apical Myosin II without changing cell volume.

We hypothesised that apical constriction may cause an expansion in basal cell size that could increase competence for capturing the basally localised ligand, and thus form part of the mechanism of competition. To investigate this, we measured the basal cell sizes of cells in areas of low and high competence for the BMP signal within the PCV field (peripheral, which may shortly lose vein fate competence, and central cells respectively) (Fig. 4D). We found that cells at the periphery often had smaller basal surfaces than those at the centre between 22 and 26 h AP, suggesting that cells which are to shortly lose their vein fate are less basally expanded (Fig. 4E–G).

To further examine whether differential basal cell size is a mechanism by which cells could compete for the BMP signal, we observed whether differences in basal cell size within the PCV field are still observed when refinement does not take place due to attenuated MyoII activity. Our data reveal that, compared to wild type wings, there are much less pronounced differences in basal cell size between central and peripheral cells when MyoII is disrupted in the posterior half of pupal wing (Supplementary Figs. 3B–C). The basal sizes associated with cells of higher competence for the BMP signal in wild type wings (central cells) are not observed when MyoII activity is disrupted. These observations are consistent with basal cell size dynamics playing a role in the mechanism of refinement.

4. Discussion

Here we found that Myosin-induced cell shape changes are coupled to the refinement of BMP signalling during PCV morphogenesis. Our findings reveal that a mechano-chemical feedback loop mediates competition for vein fate-determining BMP signalling, with less competitive cells instead acquiring intervein cell fate. Therefore, different competence for the BMP signal leads to differential cell fate determination (vein or intervein) in later pupal development. We infer that cells within the PCV field with higher levels of signalling are both more readily able to change shape and able to outcompete neighbours for the BMP signal during PCV development. Furthermore, our data provide evidence that ectopic induction of BMP signalling by expression of Tkv^{QD} results in apical Myosin II accumulation, apical constriction and cells becoming super-competent for the BMP signal, outcompeting PCV field cells that normally retain BMP signalling throughout the refinement period and causing BMP signalling to be lost in a non-cell autonomous manner (Figs. 3I and 5).

Previous studies have proposed that changes in BMP signalling induce cell competition to instruct cells for survival and elimination in the *Drosophila* wing imaginal disc (Adachi-Yamada and O'Connor, 2002; Moreno and Basler, 2004; Moreno et al., 2002). Since BMP signalling is one of the key players regulating cell proliferation in the larval wing imaginal disc (Affolter and Basler, 2007; Restrepo et al., 2014), cells lacking BMP signalling are less proliferative than neighbouring cells and are eliminated as loser cells (Bowling et al., 2019). Although BMP still serves as a proliferative signal in the *Drosophila* wing during the early pupal stage (Gui et al., 2019; Milan et al., 1996), BMP functions as a cell differentiation factor by the beginning of the refinement period. Unlike fitness-sensing cell competition, changes in BMP signalling in the pupal wing lead to an alternative cell fate path (vein or intervein) rather than survival. Although our observations do not satisfy the definition of cell competition (Nagata and Igaki, 2018), the following observations indicate that some form of competition between cells does occur. First, when
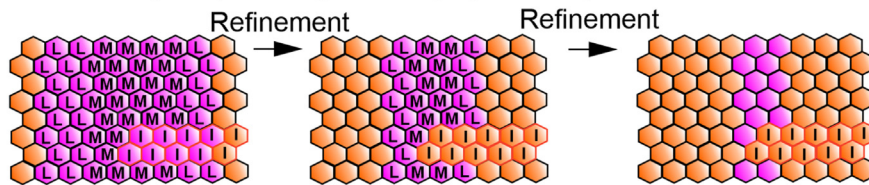
A Wild-type - competition for BMP signal
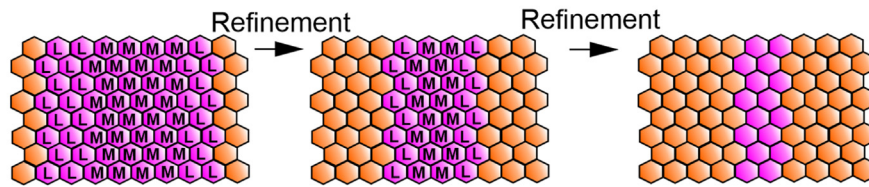
B Loss of MyoII (homogeneous population) - no competition
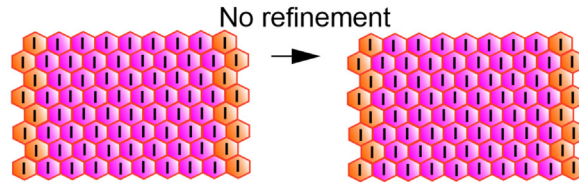
C Loss of MyoII (heterogenous population) - loss of vein fate in MyoII-DN cells

D Tkv^QD clone - super competition
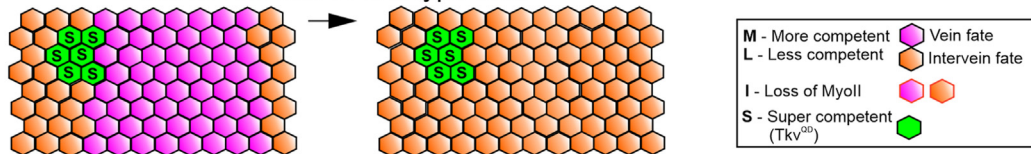### Loss of vein fate in wild type cells

Fig. 5. Schematic showing competition for BMP signal during PCV patterning in homogenous and heterogenous populations. (A) During wild type patterning, competition between PCV field cells that are more (M) and less (L) competent for BMP signalling results in progressive refinement. (B) Loss of MyoII activity and cell shape change throughout the PCV blocks refinement as no competition occurs. (C) Clones of cells with a loss of MyoII activity and cell shape change can lose their vein-fate competence as they are outcompeted by wild type neighbours (D) Super-competitive, Tkv^QD-expressing clones lose BMP signalling in the PCV region in a non-autonomous manner, resulting in loss of PCV cell fate.

cells throughout the PCV have low competence, many BMP-positive cells retain their signalling state (Figs. 3D and 5B). Second, small clones of cells less competent than neighbouring cells often lose the signal in an autonomous manner (Figs. 3G and 5C). Third, clones of super-competent cells outcompete neighbouring wild-type cells for the signal in a non-autonomous manner (Figs. 3I and 5D). Importantly, a simple feedback mechanism alone is not sufficient for explaining all these observations. Therefore, we propose that our data demonstrates "mechano-chemical feedback mediated competition for the developmental signal", a novel mechanism that might be commonly utilized during pattern formation.

The cellular mechanisms as to how cell shape changes convey higher competence for BMP signalling are not entirely clear. It is unlikely that extracellular factors that affect Dpp ligand transport (such as Cv and Sog) are direct candidates, as cells expressing MyoII-DN in the PCV region are either positive or negative for the BMP signal in a context-dependent manner that cannot be explained by disrupted Dpp transport. Our observation is consistent with the importance of basal expansion of PCV field cells for competition and refinement. PCV field cells are more basally expanded than BMP negative neighbours (Fig. 4A and B), and peripheral cells within the field (with low competence for vein fate) are less basally expanded than higher competence central cells (Fig. 4G). When competition does not occur, due to MyoII-DN expression across the

posterior wing, cells with high basal expansion are also not observed (Supplemental Figs. 3B and C). Taken together, these observations support the idea that competition and the mechano-chemical feedback loop are at least partially mediated by basal expansion. Since Tkv is observed at the basal compartment in the PCV region (Gui et al., 2016), basal expansion could integrate into BMP signalling level by either making more receptor available or by increasing receptor turnover. Alternatively basal expansion could confer higher competence to cells irrespective of receptor level, simply by allowing cells to occupy more space within a finite signalling micro-environment.

We propose that cell shape coupled competition for signalling is likely to be a general mechanism for self-organisation of pattern refinement during development. Cell shape changes are a common part of the morphogenesis programme and could feed back into developmental patterning in a variety of contexts (Gilmour et al., 2017; Hannezo and Heisenberg, 2019). Apical constriction and basal expansion are an important aspect of epithelial folding, a process which has broadly been linked to cell fate decisions and developmental patterning (Gilmour et al., 2017; Hannezo and Heisenberg, 2019; Heer and Martin, 2017; Sivakumar and Kurpios, 2018). Our finding that cell shape changes within the 2D epithelial layer, irrespective of epithelial folding, can instruct pattern refinement provides a novel insight into epithelial morphogenesis.

When MyoII activity is altered throughout the posterior wing, we

observe that the adult wing phenotypes show disrupted vein structure with thickenings and ectopic branches, rather than simply PCV expansion, as would be expected from the pMad pattern (Fig. 3F, Supplemental Fig. 2C). This may indicate that there are additional pathways to regulate or canalise vein fate specification that occur after 28h AP, once Dpp ligand is expressed autonomously. A branched PCV is a common phenotype when disrupting gene expression in the *Drosophila* wing; our findings indicate that it is possible that such observations are due to disrupted refinement of BMP signalling.

In summary, our data reveal that Myosin II-induced cell shape changes are coupled to refinement of the signalling pattern by facilitating competition between cells for signalling pathway activation. We have uncovered that competition for BMP signalling occurs via a mechano-chemical feedback loop between cell shape changes and BMP signalling, leading to self-organising refinement of the developmental field during pattern formation.

Declaration of competing interest

The authors declare no conflict of interest.

Acknowledgments

Appendix A. Supplementary data

Supplementary data to this article can be found online at https://doi.org/10.1016/j.ydbio.2021.09.006.

Author contributions

D.T-M. and O.S. conceived the project and planned experiments. D.T-M., M.P.M., N.V.T. and H.A. performed experiments. D.T-M., M.P.M., N.V.T., E.M.B. and H.A. analysed the results and discussed them with O.S. I.S–C. provided inputs. D.T-M. and O.S. wrote the manuscript and all authors made comments. O.S. supervised the project.

References

Adachi-Yamada, T., O'Connor, M.B., 2002. Morphogenetic apoptosis: a mechanism for correcting discontinuities in morphogen gradients. Dev. Biol. 251, 74–90.

Affolter, M., Basler, K., 2007. The Decapentaplegic morphogen gradient: from pattern formation to growth regulation. Nat. Rev. Genet. 8, 663–674.

Ashburner, M., Golic, K.G., Hawley, R.S., 2004. Drosophila: A Laboratory Handbook, second ed. Cold Spring Habor Press, Cold Sprig Habor, NY.

Bowling, S., Lawlor, K., Rodriguez, T.A., 2019. Cell Competition: the Winners and Losers of Fitness Selection, 146. Development.

Daniel, E., Daude, M., Kolotuev, I., Charish, K., Auld, V., Le Borgne, R., 2018. Coordination of septate junctions assembly and completion of cytokinesis in proliferative epithelial tissues. Curr. Biol. 28, 1380–1391 e1384.

Ferreira, T., Hiner, M., Rueden, C., Miura, K., Eglinger, J., Chef, B., 2017. Tferr/Scripts: BAR 1.5.1. Zenodo. https://doi.org/10.5281/zenodo.495245.

Franke, J.D., Montague, R.A., Kiehart, D.P., 2005. Nonmuscle myosin II generates forces that transmit tension and drive contraction in multiple tissues during dorsal closure. Curr. Biol. 15, 2208–2221.

Fristrom, D., Wilcox, M., Fristrom, J., 1993. The distribution of PS integrins, laminin A and F-actin during key stages in Drosophila wing development. Development 117, 509–523.

Gilmour, D., Rembold, M., Leptin, M., 2017. From morphogen to morphogenesis and back. Nature 541, 311–320.

Gui, J., Huang, Y., Montanari, M., Toddie-Moore, D., Kikushima, K., Nix, S., Ishimoto, Y., Shimmi, O., 2019. Coupling between dynamic 3D tissue architecture and BMP morphogen signaling during Drosophila wing morphogenesis. Proc. Natl. Acad. Sci. U. S. A. 116, 4352–4361.

Gui, J., Huang, Y., Shimmi, O., 2016. Scribbled optimizes BMP signaling through its receptor internalization to the Rab5 endosome and promote robust epithelial morphogenesis. PLoS Genet. 12, e1006424.

Hannezo, E., Heisenberg, C.P., 2019. Mechanochemical feedback loops in development and disease. Cell 178, 12–25.

Heer, N.C., Martin, A.C., 2017. Tension, contraction and tissue morphogenesis. Development 144, 4249–4260.

Kondo, T., Hayashi, S., 2015. Mechanisms of cell height changes that mediate epithelial invagination. Dev. Growth Differ. 57, 313–323.

Lee, T., Luo, L., 1999. Mosaic analysis with a repressible cell marker for studies of gene function in neuronal morphogenesis. Neuron 22, 451–461.

Maartens, A., 2012. Intercellular Signalling, Cell Fate and Cell Shape in the Drosophila Pupal Wing. Doctoral thesis (DPhil). University of Sussex.

Martin, A.C., Goldstein, B., 2014. Apical constriction: themes and variations on a cellular mechanism driving morphogenesis. Development 141, 1987–1998.

Matsuda, S., Blanco, J., Shimmi, O., 2013. A feed-forward loop coupling extracellular BMP transport and morphogenesis in Drosophila wing. PLoS Genet. 9, e1003403.

Matsuda, S., Shimmi, O., 2012. Directional transport and active retention of Dpp/BMP create wing vein patterns in Drosophila. Dev. Biol. 366, 153–162.

Milan, M., Campuzano, S., Garcia-Bellido, A., 1996. Cell cycling and patterned cell proliferation in the Drosophila wing during metamorphosis. Proc. Natl. Acad. Sci. U. S. A. 93, 11687–11692.

Mitonaka, T., Muramatsu, Y., Sugiyama, S., Mizuno, T., Nishida, Y., 2007. Essential roles of myosin phosphatase in the maintenance of epithelial cell integrity of Drosophila imaginal disc cells. Dev. Biol. 309, 78–86.

Morelli, L.G., Uriu, K., Ares, S., Oates, A.C., 2012. Computational approaches to developmental patterning. Science 336, 187–191.

Moreno, E., Basler, K., 2004. dMyc transforms cells into super-competitors. Cell 117, 117–129.

Moreno, E., Basler, K., Morata, G., 2002. Cells compete for decapentaplegic survival factor to prevent apoptosis in Drosophila wing development. Nature 416, 755–759.

Nagata, R., Igaki, T., 2018. Cell competition: emerging mechanisms to eliminate neighbors. Dev. Growth Differ. 60, 522–530.

Ollion, J., Cochennec, J., Loll, F., Escude, C., Boudier, T., 2013. TANGO: a generic tool for high-throughput 3D image analysis for studying nuclear organization. Bioinformatics 29, 1840–1841.

Ralston, A., Blair, S.S., 2005. Long-range Dpp signaling is regulated to restrict BMP signaling to a crossvein competent zone. Dev. Biol. 280, 187–200.

Rauzi, M., Lenne, P.F., Lecuit, T., 2010. Planar polarized actomyosin contractile flows control epithelial junction remodelling. Nature 468, 1110–1114.

Restrepo, S., Zartman, J.J., Basler, K., 2014. Coordination of patterning and growth by the morphogen DPP. Curr. Biol. 24, R245–R255.

Ross, J.J., Shimmi, O., Vilmos, P., Petryk, A., Kim, H., Gaudenz, K., Hermanson, S., Ekker, S.C., O'Connor, M.B., Marsh, J.L., 2001. Twisted gastrulation is a conserved extracellular BMP antagonist. Nature 410, 479–483.

Schindelin, J., Arganda-Carreras, I., Frise, E., Kaynig, V., Longair, M., Pietzsch, T., Preibisch, S., Rueden, C., Saalfeld, S., Schmid, B., Tinevez, J.Y., White, D.J., Hartenstein, V., Eliceiri, K., Tomancak, P., Cardona, A., 2012. Fiji: an open-source platform for biological-image analysis. Nat. Methods 9, 676–682.

Schweisguth, F., Corson, F., 2019. Self-Organization in pattern formation. Dev. Cell 49, 659–677.

Shimada, Y., Yonemura, S., Ohkura, H., Strutt, D., Uemura, T., 2006. Polarized transport of Frizzled along the planar microtubule arrays in Drosophila wing epithelium. Dev. Cell 10, 209–222.

Shimmi, O., Newfeld, S.J., 2013. New insights into extracellular and post-translational regulation of TGF-beta family signalling pathways. J. Biochem. 154, 11–19.

Shimmi, O., Ralston, A., Blair, S.S., O'Connor, M.B., 2005. The crossveinless gene encodes a new member of the Twisted gastrulation family of BMP-binding proteins which, with Short gastrulation, promotes BMP signaling in the crossveins of the Drosophila wing. Dev. Biol. 282, 70–83.

Sivakumar, A., Kurpios, N.A., 2018. Transcriptional regulation of cell shape during organ morphogenesis. J. Cell Biol. 217, 2987–3005.